ACS APPLIED MATERIALS & INTERFACES

Research Article

www.acsami.org

Dual-Ratiometric Fluorescent Nanoprobe for Visualizing the Dynamic Process of pH and Superoxide Anion Changes in Autophagy and Apoptosis

Limin Yang, Yuanyuan Chen, Zhengze Yu, Wei Pan, Hongyu Wang, Na Li,* and Bo Tang*

College of Chemistry, Chemical Engineering and Materials Science, Collaborative Innovation Center of Functionalized Probes for Chemical Imaging in Universities of Shandong, Key Laboratory of Molecular and Nano Probes, Ministry of Education, Institute of Molecular and Nano Science, Shandong Normal University, Jinan 250014, P. R. China

Supporting Information

ABSTRACT: Autophagy and apoptosis are closely associated with various pathological and physiological processes in cell cycles. Investigating the dynamic changes of intracellular active molecules in autophagy and apoptosis is of great significance for clarifying their inter-relationship and regulating mechanism in many diseases. In this study, we develop a dual-ratiometric fluorescent nanoprobe for quantitatively differentiating the dynamic process of superoxide anion ($O_2^{\bullet-}$) and pH changes in autophagy and apoptosis in HeLa cells. A rhodamine B-loaded mesoporous silica core was used as the reference, and fluorescence probes for pH and $O_2^{\bullet-}$ measurement were doped in the outer layer shell of SiO_2. Then, chitosan and triphenylphosphonium were modified on the surface of SiO_2. The experimental results showed that the nanoprobe is able to simultaneously and precisely visualize the changes of mitochondrial $O_2^{\bullet-}$ and pH in HeLa cells. The kinetics data revealed that the changes of pH and $O_2^{\bullet-}$ during autophagy and apoptosis in HeLa cells were significantly different. The pH value was decreased at the early stage of apoptosis and autophagy, whereas the $O_2^{\bullet-}$ level was enhanced at the early stage of apoptosis and almost unchanged at the initial stage of autophagy. At the late stage of apoptosis and autophagy, the concentration of $O_2^{\bullet-}$ was increased, whereas the pH was decreased at the late stage of autophagy and almost unchanged at the late stage of apoptosis. We hope that the present results provide useful information for studying the effects of $O_2^{\bullet-}$ and pH in autophagy and apoptosis in various pathological conditions and diseases.

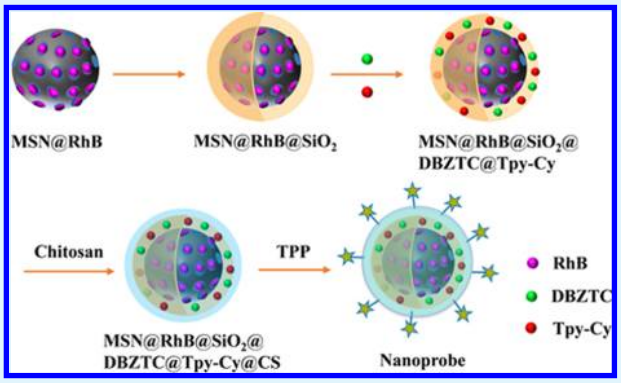

KEYWORDS: *dual-ratiometric, nanoprobe, dynamic process, superoxide anion, pH, autophagy, apoptosis*

INTRODUCTION

Autophagy ("self-eating") and apoptosis ("self-killing") are two self-destructive cell processes. Autophagy is a lysosomal degradation process to provide adenosine triphosphate under starvation conditions for maintaining nutrients and energy.[1,2] Apoptosis is the best described form of programmed cell death, which is critical for maintaining cellular homeostasis.[3] Autophagy and apoptosis are closely related to various pathological conditions and diseases.[4−7] Also, their functional relationship is complex in these diseases.[8] Consequently, the variations of intracellular active molecules during autophagy and apoptosis processes have received extensive attention because these will be of help for investigating their inter-relationship and regulating mechanism in these diseases.[9,10] It has been found that the variations of pH and $O_2^{\bullet-}$ were commonly accompanied with autophagy and apoptosis.[11−14] In most of these studies, they only detect pH or $O_2^{\bullet-}$ changes in autophagy or apoptosis processes separately. However, the dynamic processes of $O_2^{\bullet-}$ and pH changes in autophagy and apoptosis have still not been investigated. Therefore, developing a fluorescent probe that can accurately quantify pH and $O_2^{\bullet-}$ changes is expected to reveal the differences between autophagy and apoptosis, which will offer useful information for studying their functional relationship in many diseases.

Recently, a series of molecular fluorescent probes and nanoprobes have been developed for determining pH or $O_2^{\bullet-}$.[15−20] Nevertheless, the fluorescence signal can be influenced by the imaging parameters, local probe concentration, etc.[21] By contrast, ratiometric fluorescent probes are favorable for quantitative detection and imaging of pH and $O_2^{\bullet-}$ because they can not only improve the accuracy of measurements but also avoid the disturbance from background fluorescence.[22] To date, many fluorescent probes have been

Received: June 8, 2017
Accepted: August 3, 2017
Published: August 3, 2017

DOI: 10.1021/acsami.7b08223
ACS Appl. Mater. Interfaces 2017, 9, 27512−27521

Scheme 1. Illustration of the Nanoprobe Formation and the Structures of RhB, DBZTC, and Tpy-Cy

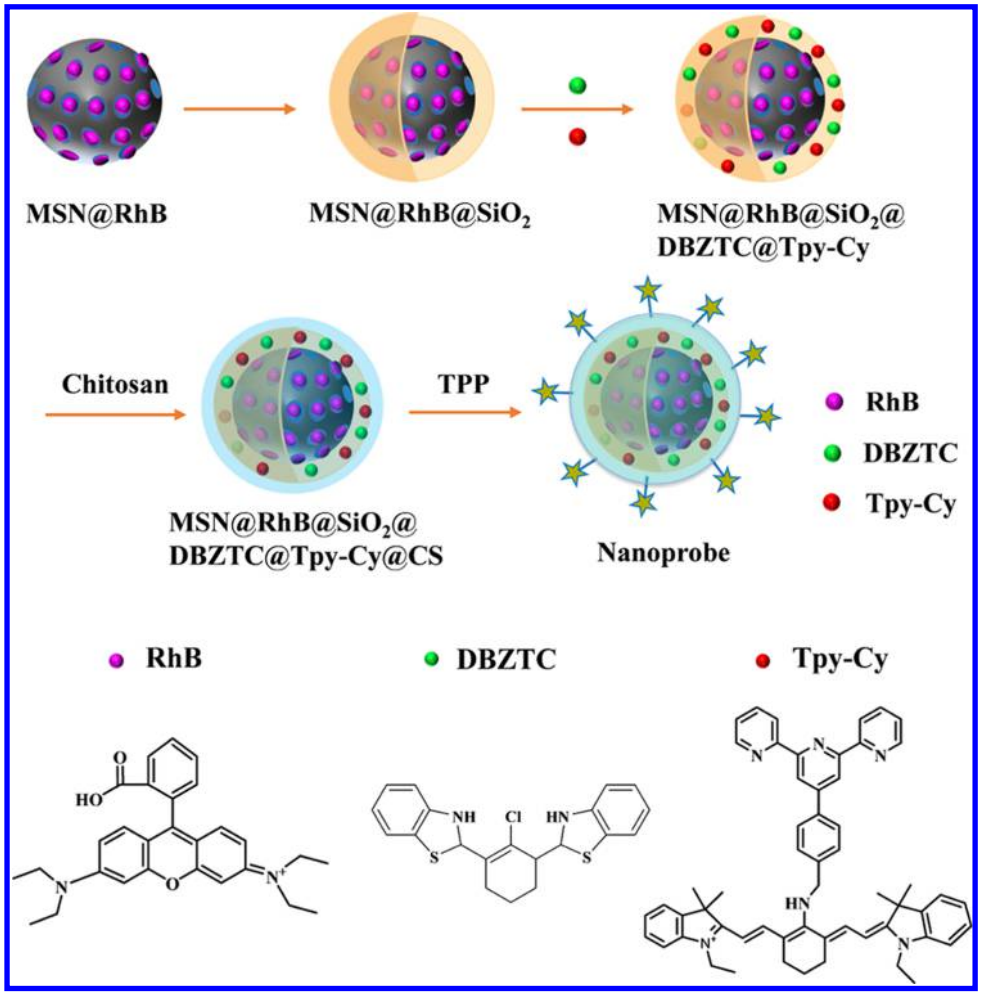

reported for ratiometric visualizing of individual pH or $O_2^{\bullet-}$ in living cells.[23−28] However, as these fluorescent probes are specific to $O_2^{\bullet-}$ or pH they are not able to simultaneously respond to $O_2^{\bullet-}$ and pH in autophagy and apoptosis processes. Thus, the development of a single probe that can achieve the real-time monitoring of the dynamic process of $O_2^{\bullet-}$ and pH changes without mutual interference in autophagy and apoptotic processes remains a major challenge.

Herein, we develop a dual-ratiometric nanoprobe for simultaneous imaging of pH and $O_2^{\bullet-}$ and further investigation of the dynamics of pH and $O_2^{\bullet-}$ variations in autophagy and apoptosis in HeLa cells. First, the mesoporous silica nanoparticle (MSN) support was loaded with rhodamine B (RhB). The RhB molecules were chosen as the reference because their fluorescence characteristics were not influenced by the pH and $O_2^{\bullet-}$. The core−shell nanoparticles MSN@RhB@SiO_2 using MSN@RhB as the core and SiO_2 as the shell were obtained via a modified Stöber sol−gel method.[29] Two molecular fluorescence probes, 2-chloro-1,3-dibenzothiazo-linecyclohexene (DBZTC) for $O_2^{\bullet-}$ measurement and 2-{4-[4′-aminomethylphenyl)-2,2′:6′,2″-terpyridinyl]-7-(1-ethyl-3,3-dimethyl-(indolin-2-ylidene)}-3,5-(propane-1,3-diyl)-1,3,5-heptatrien-1-yl)-1-ethyl-3,3-dimethyl-3*H*-indolium (Tpy-Cy) for pH detection,[30,31] were then doped in the outer layer shell of SiO_2. To avoid the leakage of the fluorescence molecules, chitosan (CS) was further coated on the surface of the SiO_2 via electrostatic effect. Subsequently, triphenylphosphonium (TPP) was covalently linked on the CS surface for mitochondria targeting in living cells. The core−shell structure-based nanoprobe shows various advantages, such as good biocompatibility, accurate sensing of two analytes, and specific mitochondria targeting. The details of the strategy are displayed in Scheme 1.

EXPERIMENTAL SECTION

Reagents and Materials. Tetraethyl orthosilicate (TEOS), reduced glutathione (GSH), ascorbic acid (VC), hypochlorite (NaOCl), sodium chloride (NaCl), triethanolamine (TEA), chitosan, hexadecyl trimethyl ammonium chloride (CTAC), 4,5-dihydroxy-1,3-benzenedisulfonic acid disodium salt (Tiron), H_2O_2, and *tert*-butylhydroperoxide (TBHP) were purchased from China National Pharmaceutical Group Corp. (Shanghai, China). Rhodamine B was purchased from Tianjin Heowns Biochemical Technology Co., Ltd. (Tianjin, China). 1-Ethyl-3-(3-dimethly-aminopropyl)carbodiimide (EDC) and (4-carboxybutyl)triphenylphosphonium bromide were obtained from Alfa Aesar Chemical Ltd. (Tianjin, China). Xanthine (XA), xanthine oxidase (XO), and 3-(4,5-dimethylthiazol-2-yl)-2,5-diphenyl tetrazolium bromide (MTT) were purchased from Sigma-Aldrich. L-Buthionine sulphoximine (BSO) was obtained from Sigma-Aldrich. Human cervical cancer cell line HeLa was purchased from Procell Life Science Co., Ltd. 2-{4-[4′-(Aminomethylphenyl)-2,2′:6′,2″-terpyridinyl]-7-(1-ethyl-3,3-dimethyl(indolin-2-ylidene)}-3,5-(propane-1,3-diyl)-1,3,5-heptatrien-1-yl)-1-ethyl-3,3-dimethyl-3*H*-indolium (Tpy-Cy) and 2-chloro-1,3-dibenzothiazo-linecyclohexene (DBZTC) were synthesized in our laboratory.[30,31] ^{1}H NMR and elemental analysis were employed to characterize Tpy-Cy. The data are consistent with the previous report and are shown as following: ^{1}H

DOI: 10.1021/acsami.7b08223
ACS Appl. Mater. Interfaces 2017, 9, 27512−27521

NMR (300 MHz, dimethyl sulfoxide (DMSO)-d_6) δ (ppm): 1.38−1.54 (m, 22H), 1.98 (s, 1H), 2.71 (s, 2H), 2.87 (s, 2H), 3.84 (s, 2H), 4.41 (d, 2H), 5.17 (s, 1H), 5.64 (s, 1H), 5.80 (m, 1H), 6.23 (m, 1H), 7.52−8.18 (m, 14H), 8.51−8.76 (m, 7H), 10.12 (s, 1H). Elemental analysis: Calcd C, 71.4; H, 6.1; I, 13.4; N, 8.93. Found C, 71.5; H, 6.1; I, 13.5; N, 8.9. ^{1}H NMR and elemental analysis were employed to characterize DBZTC. The data are consistent with the previous report and are shown as following: ^{1}H NMR (300 MHz, DMSO-d_6, 25 °C, tetramethylsilane): δ 8.10−7.90 (m, 2H, benzol-H), 7.75 (d, 2H, benzol-H), 7.47−7.39 (m, 2H, benzol-H), 7.24 (d, 2H, benzol-H), 4.10 (m, 2H, N−H), 3.12 (m, 2H, methine-H), 2.3 (m, 3H, cyclohexene-H), 1.15 (m, 4H, cyclohexene-H). Elemental analysis: Calcd C, 62.10; H, 4.92; N, 7.24. Found C, 62.02; H, 4.84; N, 7.36. All chemicals were of analytical grade. Doubly distilled water was used in all experiments.

Apparatus. High-resolution transmission electron microscopy (TEM) was performed on a JEM-2100 electron microscope, using an accelerating voltage of 200 kV. Fluorescence spectra measurements were carried out on an FLS-980 Edinburgh Fluorescence Spectrometer. Confocal fluorescence imaging experiments were carried out on a TCS SP5 (Leica Co., Ltd., Germany) confocal laser-scanning microscope. MTT assay was recorded using a microplate reader (Synergy 2; BioTek Instruments, Inc.).

Synthesis of Mesoporous Silica@Rhodamine B@Silica Nanoparticle (MSN@RhB@SiO$_2$). For the synthesis of the MSN,[32] 0.5 g of CTAC and 0.08 g of TEA were dissolved in 20 mL of doubly distilled water. Then, 1.5 mL of TEOS was added dropwise and stirred for another 1 h at 95 °C. The product was washed with methanol several times. Subsequently, the collected precipitates were extracted for 12 h with a 1 wt % solution of NaCl in methanol at 35 °C. The extraction was performed several times with the aim of removing the template CTAC.

For the synthesis of the MSN@RhB, 20 mg of MSN was added to 10 mL of RhB solution (0.5 mg/mL) and stirred for 24 h to allow encapsulation of RhB by MSN. After this procedure, the RhB-loaded MSN particles were separated by centrifugation. The as-prepared nanoparticles are denoted as MSN@RhB. Then, the obtained MSN@RhB was dispersed in 20 mL of water and 8 mL of ethanol under stirring. Ammonia aqueous solution (0.2 mL, 28 wt %) was added to the above solution. Subsequently, 0.3 mL of TEOS was added dropwise to the solution with rapid stirring. The mixture was stirred for 12 h at 30 °C in darkness. After the reaction, the product was collected and washed several times by centrifugation with ethanol and water. The as-prepared nanoparticles are denoted as MSN@RhB@SiO$_2$.

Preparation of the Nanoprobe. MSN@RhB@SiO$_2$ (2 mg) was dispersed in water (2 mL). Then, Tpy-Cy (0.5 mM) and DBZTC (0.2 mM) were added and the mixture was stirred for 12 h at room temperature. Subsequently, chitosan was added and stirred for another 12 h. To identify the influence of chitosan content on DBZTC and Tpy-Cy leakage, varied concentrations of chitosan (0.02, 0.05, 0.1, 0.2, 0.4, and 0.6 mg/mL) were added to MSN@RhB@SiO$_2$@Tpy-Cy@DBZTC solution. When the concentration of chitosan reached 0.2 mg/mL, the leakage amount was not changed any more (data are not shown). Therefore, 0.2 mg/mL chitosan was used in subsequent experiments. The nanoparticles were centrifuged and repeatedly washed with water. The obtained nanoparticles are denoted as MSN@RhB@SiO$_2$@Tpy-Cy@DBZTC@CS. Because chitosan has a lot of amino groups, TPP can be covalently conjugated onto the surface of nanoparticles by the formation of the amido bond. In this work, 1 mM TPP was dissolved in 2-morpholinoethanesulfonic acid solution (pH 6.0), followed by the addition of 3 mM EDC. The mixture was then stirred for 30 min to activate the carboxylic group of TPP. Subsequently, MSN@RhB@SiO$_2$@Tpy-Cy@DBZTC@CS was added to the above solution and stirred for 12 h. Excess EDC and TPP were removed by repeatedly washing the nanoparticles with distilled water. MSN@RhB@SiO$_2$@CS-TPP was also prepared using the same procedure, except without Tpy-Cy and DBZTC.

Spectrophotometric Measurements. To quantify the amount of DBZTC and Tpy-Cy in the nanoprobe, 1 mL of nanoprobe solution (0.2 mg/mL) was heated at 70 °C for 1 h. The supernatant solution was collected by centrifugation. The fluorescence intensity of the supernatant was measured. The concentrations of DBZTC and Tpy-Cy were quantified on the basis of the calibration curve of DBZTC and Tpy-Cy, respectively. To evaluate the TPP-modifying efficiency, the supernatant was collected. The concentration of TPP can be determined according to the calibration curve of TPP. The content of TPP on the nanoprobe was calculated by the initial amount of TPP added into the solution subtracted by the amount of TPP in the supernatant.

To evaluate the RhB-loading capacity, 1 mL of MSN@RhB@SiO$_2$ (0.2 mg/mL) solution was heated at 70 °C for 1 h. The supernatant solution was collected by centrifugation. The fluorescence intensity of the supernatant at 575 nm was measured. The loading efficiency of RhB in MSN@RhB@SiO$_2$ was calculated according to a calibration curve of RhB.

The concentration of the nanoprobe was 0.2 mg/mL for the determination of $O_2^{\bullet-}$ and pH. For the detection of $O_2^{\bullet-}$, we applied XA/XO as the source of $O_2^{\bullet-}$. One unit of XO can catalyze the conversion of 1.0×10^{-6} mol XA into 0.33×10^{-6} mol $O_2^{\bullet-}$. Different concentrations of XA/XO were added to the reaction solution and incubated at 37 °C for 10 min. The fluorescence intensity of DBZTC and RhB were measured at $\lambda_{ex}/\lambda_{em}$ = 470/527 nm and $\lambda_{ex}/\lambda_{em}$ = 560/575 nm, respectively. For the detection of pH, different pH buffer solutions were prepared by using 10 mM *N*-(2-hydroxyethyl)-piperazine-*N*′-ethanesulfonic acid (HEPES). The fluorescence intensities of Tpy-Cy and RhB were collected with $\lambda_{ex}/\lambda_{em}$ = 650/750 nm and $\lambda_{ex}/\lambda_{em}$ = 560/575 nm, respectively.

Interference Study. To evaluate the selectivity of the nanoprobe toward $O_2^{\bullet-}$, the effect of other reactive oxygen species and biological compounds (•OH) were tested. Hydroxyl radical (•OH) was prepared by the reaction of H_2O_2 with Fe^{2+}. Nitric oxide (NO) was obtained from 3-morpholinosydnonimine hydrochloride. Singlet oxygen ($^1O_2$) was generated through the reaction of ClO^- with H_2O_2. To evaluate the selectivity toward H^+, metal ions (Cu^{2+}, Fe^{2+}, Mn^{2+}, Zn^{2+}, Co^{2+}, Ca^{2+}, Mg^{2+}, K^+, and Na^+) were examined. The oxidative-stress-associated redox chemicals, including H_2O_2 and glutathione, were also tested.

Cytotoxicity Assay. The cytotoxicity of the nanoprobe was investigated by the standard MTT assay. Briefly, HeLa cells were dispersed within 96-well microtiter plates and incubated with the nanoprobe at different concentrations (0.2, 0.4, and 0.8 mg/mL) for 12 and 24 h. MTT solution (0.5 mg/mL in phosphate-buffered saline (PBS)) was then added to each well. The MTT solution was abandoned after 4 h. Subsequently, 150 μL of DMSO was added to each well. Absorbance values of the wells were measured at 490 nm.

Cell Culture and Imaging. HeLa cells were cultured in RPMI-1640 medium supplemented with 10% fetal bovine serum (WelGene), penicillin (100 units/mL), and streptomycin (100 μg/mL). All cells were maintained in a humidified atmosphere of at 37 °C. The nanoprobe (0.2 mg/mL) was delivered into the cells for 12 h at 37 °C in 5% CO_2. In colocalization experiments, the cells were treated and incubated with 0.2 mg/mL MSN@RhB@SiO$_2$@CS-TPP or MSN@RhB@SiO$_2$@CS for 12 h, washed with PBS, then incubated with MitoTracker Green (MTG) or LysoTracker Green (LTG) (50 nM). The excitation wavelength of LTG and MTG was 488 nm, the collection window was 500−550 nm. The excitation wavelength of MSN@RhB@SiO$_2$@CS or MSN@RhB@SiO$_2$@CS-TPP was 543 nm, and the collection window was 555−620 nm.

The ratiometric imaging of mitochondrial $O_2^{\bullet-}$ of the nanoprobe in living cells was performed as follows. HeLa cells were incubated with the nanoprobe or incubated with the nanoprobe and then stimulated with 2-methoxyestradiol (2-ME) (5 μg/mL) for 1 h or stimulated with 2-ME (5 μg/mL) for 1 h and then treated with Tiron (100 μM) for 30 min and then incubated with the nanoprobe. The pH sensing was performed in the nanoprobe-loaded HeLa cell incubated with high K^+ buffer and ionophore nigericin (10 μM). High K^+ buffer with different pH values were prepared with 30 mM NaCl, 120 mM KCl, 0.5 mM $MgSO_4$, 1 mM NaH_2PO_4, 1 mM $CaCl_2$, 20 mM HEPES, and 5 mM glucose. The nanoprobe-loaded HeLa cells in PBS (pH 7.4) as intact

DOI: 10.1021/acsami.7b08223
ACS Appl. Mater. Interfaces 2017, 9, 27512−27521

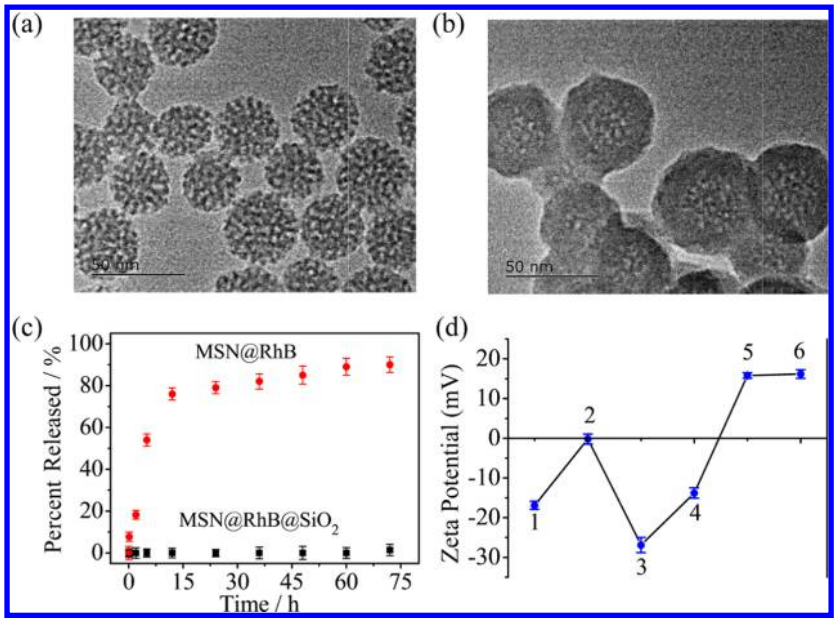

Figure 1. TEM images of MSN (a) and MSN@RhB@SiO_2 (b). (c) The leakage of RhB from RhB@MSN and RhB@MSN@SiO_2. (d) Zeta potential of the every-step modification: (1) MSN, (2) MSN@RhB, (3) MSN@RhB@SiO_2, (4) MSN@RhB@SiO_2@Tpy-Cy@DBZTC, (5) MSN@RhB@SiO_2@Tpy-Cy@DBZTC@CS, and (6) nanoprobe.

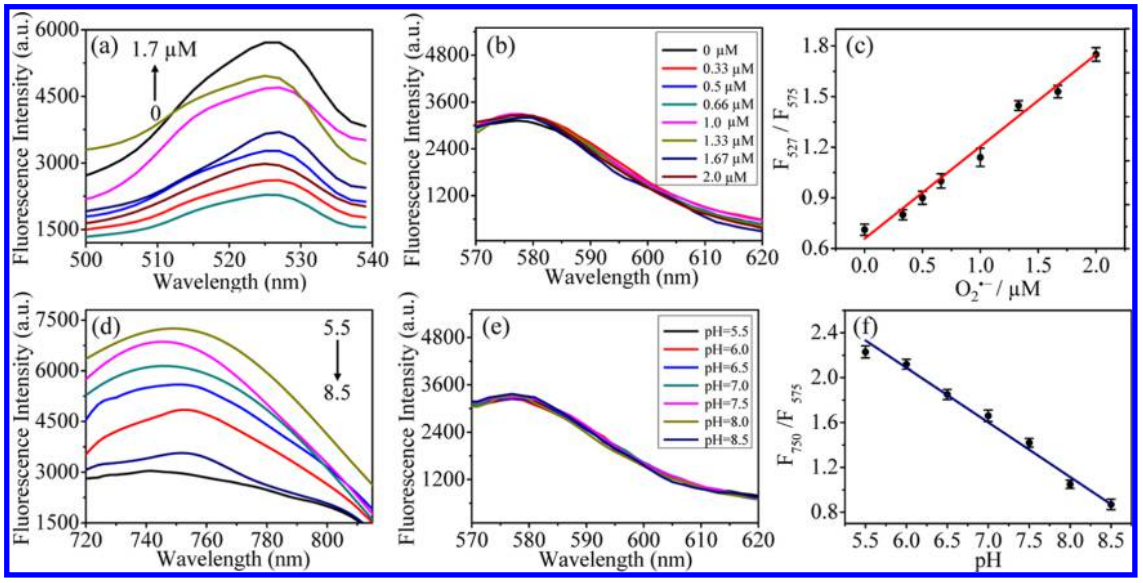

Figure 2. Fluorescence response of the nanoprobe towards different concentrations of $O_2^{\bullet-}$ under 470 nm excitation (a) and 560 nm excitation (b). (c) The fluorescence intensity ratio F_{527}/F_{575} as a function of $O_2^{\bullet-}$. Fluorescence response of the nanoprobe with various pH values under 650 nm excitation (d) and 560 nm excitation (e). (f) The fluorescence intensity ratio F_{750}/F_{575} as a function of pH. The concentration of the nanoprobe was 0.2 mg/mL.

cells were directly subjected to fluorescence imaging. The excitation wavelength of the green channel (DBZTC) was 488 nm and the collection window was 500−550 nm. The excitation wavelength of the purple channel (RhB) was 543 nm and the collection window was 555−620 nm. The excitation wavelength of the red channel (Tpy-Cy) was 633 nm and the collection window was 645−750 nm. The green/purple channel and red/purple channel were the pseudocolored ratiometric images. Other information is available in the figure captions. The fluorescence intensity of cells (at least 50 cells) was the average fluorescence intensity from the confocal fluorescence images. Then, the ratio of F_{green}/F_{Purple} was obtained by the green average fluorescence intensity divided by the purple average fluorescence intensity. The ratio of F_{red}/F_{Purple} was also obtained by the same method. For the autophagy and apoptosis experiments, HeLa cells were treated with the nanoprobe (0.2 mg/mL) for 12 h and then washed with PBS three times. For the autophagy experiments, a glyphosate (GP)-starvation medium was added to induce the autophagy process for different times. To study the formation of acidic vesicular organelles (AVOs), starvation-treated HeLa cells with different times were then incubated with acridine orange (100 μg/mL) for 5 min to observe the formation of acidic vesicular organelles. For the apoptosis experiments, the nanoprobe-treated HeLa cells were incubated with BSO (5 mM) for various times to induce cell apoptosis. Cell imaging was performed after washing cells with PBS. To investigate the changes of the mitochondrial membrane potential ($\Delta\psi_m$), HeLa cells first were treated with BSO (5 mM) for various times and then incubated with rhodamine 123 (5 μg/mL) for 15 min.

DOI: 10.1021/acsami.7b08223
ACS Appl. Mater. Interfaces 2017, 9, 27512−27521

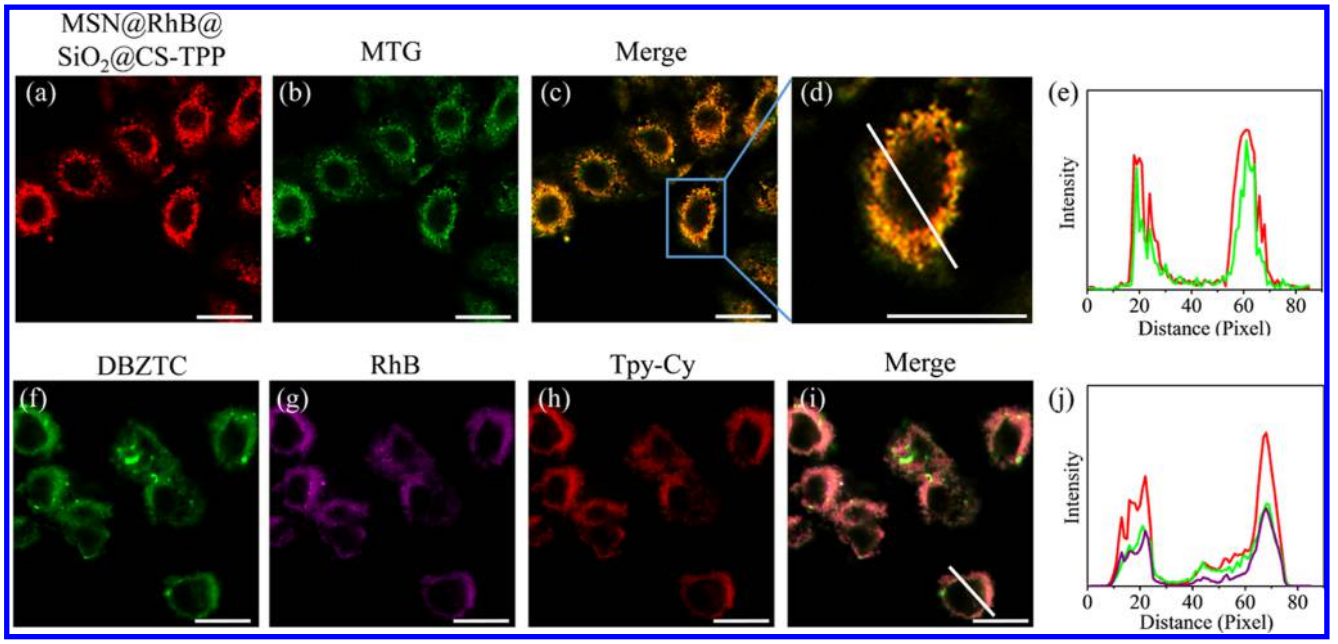

Figure 3. Confocal images of HeLa cells incubated with MSN@RhB@SiO_2@CS-TPP (a) and MTG (b). (c) The merged image of (a) and (b). (d) The enlarged image from the square marked in image (c). (e) The intensity profile of white line in image (d). Confocal images of HeLa cells incubated with nanoprobe. (f–h) The confocal images of DBZTC, RhB, and Tpy-Cy of the nanoprobe. (i) The merged image of (f)–(h). (j) The intensity profile of white line in image (i). The excitation wavelength of DBZTC and MTG were 488 nm. The excitation wavelength of RhB and Tpy-Cy were 543 and 633 nm, respectively. Scale bars: 100 μm.

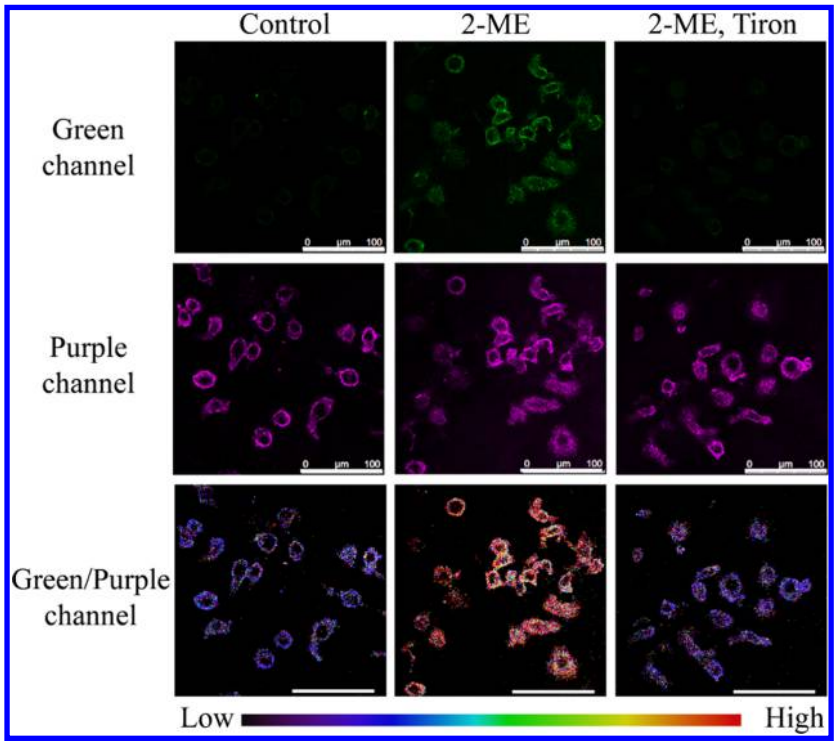

Figure 4. Fluorescent images of HeLa cells incubated with the nanoprobe or incubated with the nanoprobe and then stimulated with 2-ME or stimulated with 2-ME, then treated with Tiron and then incubated with nanoprobe. The concentration of the nanoprobe was 0.2 mg/mL. The excitation wavelengths of the green channel (DBZTC) and purple channel (RhB) are 488 and 543 nm, respectively. The green/purple channel is shown the pseudocolored ratiometric images. Scale bars: 100 μm.

RESULTS AND DISCUSSION

Design and Synthesis of the Nanoprobe. As shown in Figure 1a, the as-prepared MSN displayed a mean size of about 30 nm. After the RhB molecules loaded into the pores of MSN, the SiO_2 layer was coated on the MSN@RhB via a modified Stöber sol–gel process.[29] The core–shell structure of MSN@RhB@SiO_2 can be observed clearly in Figure 1b. The average diameter of MSN@RhB@SiO_2 was about 50 nm with the SiO_2 shell thickness of around 10 nm. Moreover, the size and hydrodynamic diameter of the nanoprobe were about 50 and

DOI: 10.1021/acsami.7b08223
ACS Appl. Mater. Interfaces 2017, 9, 27512–27521

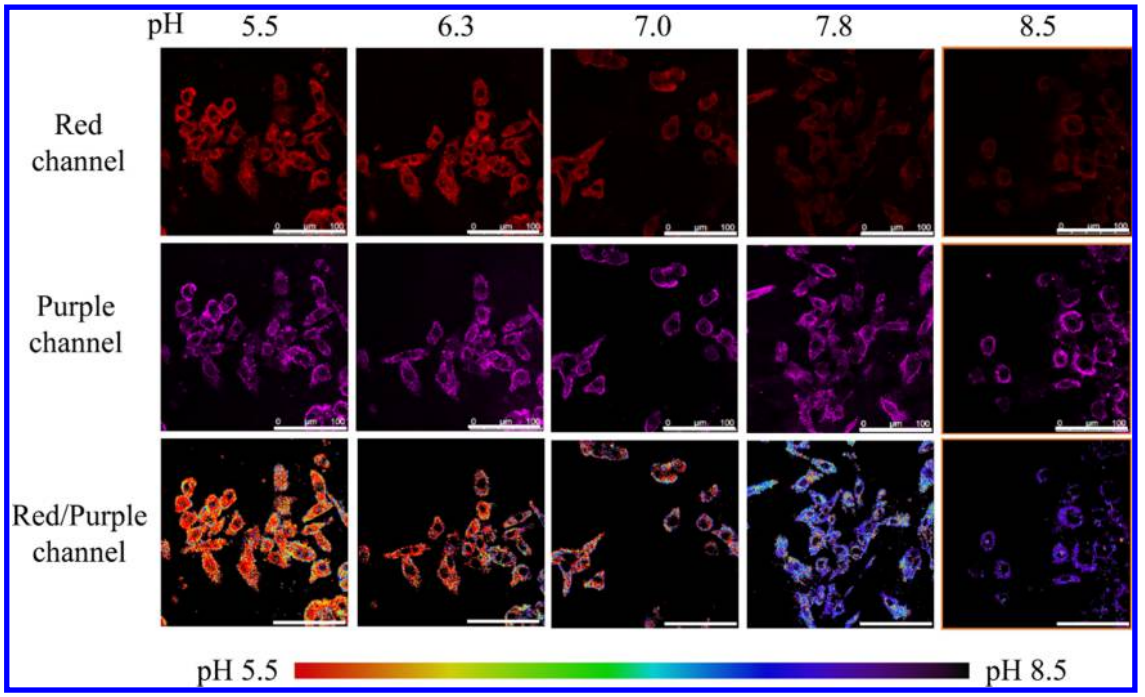

Figure 5. Fluorescent images of HeLa cells treated with the nanoprobe at different pH. The concentration of the nanoprobe was 0.2 mg/mL. The excitation wavelengths of the purple channel (RhB) and red channel (Tpy-Cy) are 543 and 633 nm, respectively. The red/purple channel is shown in the pseudocolored ratiometric images. Scale bars: 100 μm.

133 nm, respectively (Figure S1). The leakage of RhB was evaluated via time-dependent fluorescence changes. As shown in Figure 1c, the RhB molecules were entrapped in MSN@SiO_2 without being released for more than 72 h compared with MSN. It strongly indicated that the SiO_2 layer could effectively prevent the RhB molecules from leaking out of the MSN mesopores.

Then, zeta potential experiments were performed to verify the successful assembling of the nanoprobe. As shown in Figure 1d, the zeta potential values of MSN, MSN@RhB, and MSN@RhB@SiO_2 were −16.8, −0.18, and −26.9 mV, respectively. After loading DBZTC and Tpy-Cy, the zeta potential increased to −13.8 mV. With further modification of CS and TPP, the zeta potential values were +15.8 and +16.2 mV, respectively. These results demonstrated that the nanoprobe was successfully prepared. Additionally, the loading contents of RhB, DBZTC, and Tpy-Cy in the nanoprobe were determined to be about 0.12, 1.0, and 11.0 mg/g, respectively (Figure S2a−c). The amount of TPP was calculated to be 8.5 mg per 1 g of the nanoprobe (Figure S2d). Further experimental results showed that the nanoprobe has good stability under continuous light illumination (Figure S3) and different ion strengths (Figure S4).

Ratiometric Detection of $O_2^{\bullet-}$ and pH. The fluorescence spectroscopic properties of the nanoprobe at different concentrations of $O_2^{\bullet-}$ and various pH values were investigated. As shown in Figure 2a, the fluorescence intensity at 527 nm enhanced gradually when the concentration of $O_2^{\bullet-}$ increased from 0 to 1.7 μM, whereas the changes of fluorescence intensity at 575 nm were negligible (Figure 2b). As a result, a good linearity was obtained on the basis of plotting the ratio of the fluorescent intensity at 527 and 575 nm (F_{527}/F_{575}) versus $O_2^{\bullet-}$ concentration (Figure 2c).

The results revealed that the nanoprobe could be considered as a ratio probe for achieving determination of $O_2^{\bullet-}$. The changes of fluorescence intensity at different pH values of the nanoprobe were further studied. Successively decreased fluorescence intensities at 750 nm were observed when the values of pH increased from 5.5 to 8.5 (Figure 2d). As expected, the fluorescence intensity at 575 nm did not change at various pH values (Figure 2e). The ratio of fluorescent intensities (F_{750}/F_{575}) displayed a good linear relationship with pH in the range of 5.5−8.5 (Figure 2f), which covers most of the pH ranges needed for biological applications. Therefore, all the results strongly illustrated that the nanoprobe could be considered as a ratio probe for simultaneously achieving determination of $O_2^{\bullet-}$ and pH.

Next, to confirm whether the nanoprobe could selectively detect $O_2^{\bullet-}$, other reactive oxygen species or relevant analytes, including $^1O_2$, OCl^-, GSH, H_2O_2, NO, •OH, $ONOO^-$, TBHP, and VC were investigated. As shown in Figure S5, these interferences did not show obvious changes compared with the control. The evident fluorescence change of the nanoprobe was witnessed in the presence of $O_2^{\bullet-}$. It implies that the nanoprobe can realize ratiometric fluorescent sensing $O_2^{\bullet-}$ without interference from other biologically relevant substances. To further investigate whether the nanoprobe could selectively detect pH, we examined interference from various biologically relevant metal ions (Cu^{2+}, Fe^{2+}, Mn^{2+}, Zn^{2+}, Co^{2+}, Ca^{2+}, Mg^{2+}, K^+, and Na^+) and biologically related redox chemicals (GSH and H_2O_2). As shown in Figure S6, no noticeable changes were observed under these conditions. This suggested that the ratiometric fluorescence response of the nanoprobe for pH was highly selective from that of other competing substances. Taken together, these results demonstrated that the developed ratiometric nanoprobe was able to selectively and simultaneously determine $O_2^{\bullet-}$ and pH.

Cytotoxicity Assay. To investigate the in vitro cytotoxicity of the nanoprobe, a standard MTT assay was performed. As shown in Figure S7, when the concentration of the nanoprobe

DOI: 10.1021/acsami.7b08223
ACS Appl. Mater. Interfaces 2017, 9, 27512−27521

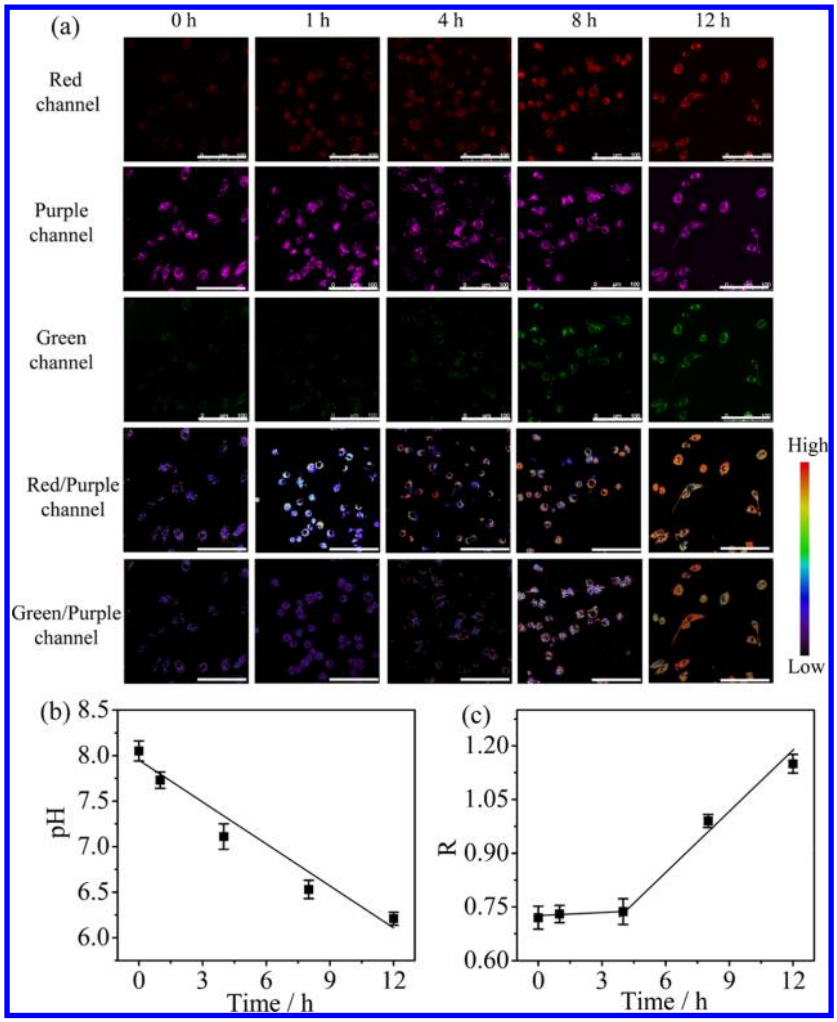

Figure 6. (a) Fluorescence imaging of nanoprobe-incubated HeLa cells treated by GP-starvation for different times. The concentration of the nanoprobe was 0.2 mg/mL. The excitation wavelength of the green channel (DBZTC), purple channel (RhB), and red channel (Tpy-Cy) are 488, 543, and 633 nm, respectively. The green/purple channel and red/purple channel are the pseudocolored ratiometric images. Scale bars: 100 μm. (b) The pH of HeLa cells treated by GP-starvation for different times. (c) The ratio values ($R = F_{Green}/F_{Purple}$) of HeLa cells treated by GP-starvation for different times.

was up to 0.8 mg/mL, the cell viabilities were more than 95% after incubation for 12 and 24 h, respectively. This suggested that the developed nanoprobe was of little toxicity in vitro. This result clearly indicated that the nanoprobe had good biocompatibility for cellular imaging.

Mitochondria-Targeting Ability Study of the Nanoprobe. To investigate whether the nanoprobe could specifically target mitochondria, costaining experiments in living cells were studied via confocal laser-scanning microscopy. MitoTracker Green (MTG) was used to stain mitochondria in HeLa cells. The nanoprobe was replaced with MSN@RhB@SiO_2@CS-TPP nanoparticles to avoid spectra overlap with MTG. As shown in Figure 3c, an obvious yellow signal was observed in the merged image, which corresponded to the colocalization of the green and red signals. Pearson's correlation coefficient was about 0.75, which demonstrated that MSN@RhB@SiO_2@CS-TPP nanoparticles exhibited excellent mitochondrial target capability. By contrast, the mitochontrial target ability of MSN@RhB@SiO_2@CS nanoparticles was also studied. As shown in Figure S8, MSN@RhB@SiO_2@CS nanoparticles exhibited inferior mitochondria targeting ability (Pearson's correlation coefficient, ρ = 0.36). These data demonstrate that the conjugation of TPP plays a decisive role in the mitochondria targeting procedure.[33] Also, the localization of the nanoprobe in lysosome was performed. The HeLa cells were stained with LysoTracker Green to label the lysosome. As shown in Figure S9, no obvious yellow signal was observed in the merged image and the Pearson's correlation coefficient was about 0.27, indicating that the MSN@RhB@SiO_2@CS-TPP nanoparticles exhibited inferior targeting ability for lysosome. Moreover, a well-merged image of DNZTC, RhB, and Tpy-Cy of the nanoprobe (Figure 3i) was further obtained. At the same time, fluorescence intensity profile results were consistent with the imaging experiments (Figure 3e,j). These results suggest that the nanoprobe has the capability to selectively target mitochondria and measure analytes at the same location of mitochondria in living cells.

Ratiometric Imaging of Mitochondrial $O_2^{\bullet-}$ and pH. The ratiometric imaging of mitochondrial $O_2^{\bullet-}$ of the nanoprobe in HeLa cells was first performed. 2-Methoxyestradiol (2-ME) was chosen to increase $O_2^{\bullet-}$ concentrations in living cells.[34] As shown in Figure 4, a faint green fluorescence signal was observed after HeLa cells were incubated with the nanoprobe. Subsequently, the strong green fluorescence signal

DOI: 10.1021/acsami.7b08223
ACS Appl. Mater. Interfaces 2017, 9, 27512−27521

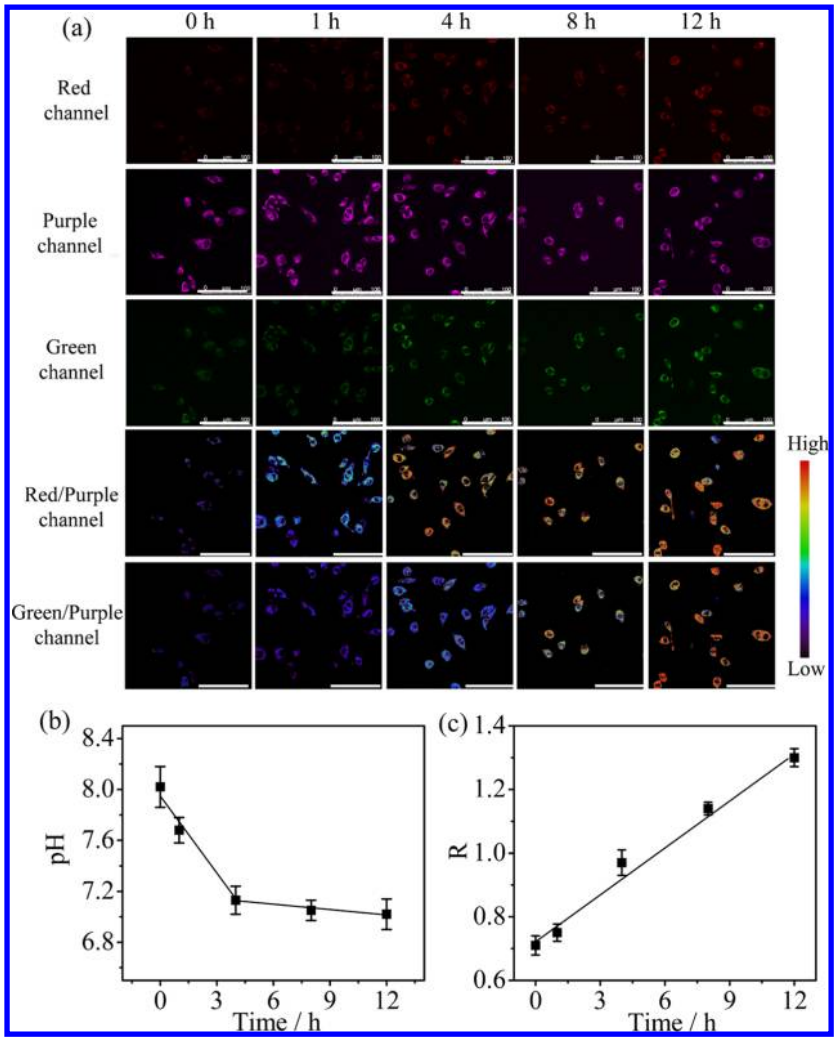

Figure 7. (a) Fluorescence imaging of nanoprobe-incubated HeLa cells treated by BSO for different times. The concentration of the nanoprobe was 0.2 mg/mL. The excitation wavelength of the green channel (DBZTC), purple channel (RhB), and red channel (Tpy-Cy) are 488, 543, and 633 nm, respectively. The green/purple channel and red/purple channel are the pseudocolored ratiometric images. Scale bars: 100 μm. (b) The pH of HeLa cells treated by BSO for different times. (c) The ratio values ($R = F_{Green}/F_{Purple}$) of HeLa cells treated by BSO for different times.

was distinctly observed in nanoprobe-incubated HeLa cells treated with 2-ME, whereas the purple fluorescence signal hardly altered. As expected, the increased average ratio value (F_{Green}/F_{Purple}) (Figure S10) was obtained by ratiometric imaging. These results indicated that the concentration of $O_2^{\bullet-}$ rose after 2-ME stimulation. Then, the green fluorescence signal significantly decreased when HeLa cells were pretreated with Tiron (a superoxide scavenger), whereas the purple fluorescence signal was not changed. Subsequently, the average ratio value of F_{Green}/F_{Purple} reduced obviously in Tiron-pretreated HeLa cells, which demonstrated that the $O_2^{\bullet-}$ concentration reduced, suggesting the nanoprobe had good specificity towards $O_2^{\bullet-}$. All of these results demonstrated the nanoprobe could be utilized for ratiometric imaging of mitochondrial $O_2^{\bullet-}$ changes.

Next, the nanoprobe was employed to sense the mitochondrial pH changes in HeLa cells. High K^+ buffer and ionophore nigericin (10 μM) were applied to change the intracellular pH.[35] Figure 5 shows that the red fluorescence emission of nanoprobe-treated HeLa cells gradually weakened upon increasing the pH from 5.5 to 8.5, whereas the purple fluorescence emission generally displayed no changes. Moreover, a good linear calibration curve was obtained between the average emission intensity ratio (F_{Red}/F_{Purple}) and pH variations in the range of 5.5−8.5 (Figure S11), implying that the nanoprobe was capable of visualizing the changes of mitochondrial pH. On the basis of this curve, the averaged pH value of mitochondria was determined to be 8.03 ± 0.16. Therefore, all of these results suggested that the developed ratiometric nanoprobe was applicable for precisely monitoring and imaging mitochondrial pH and $O_2^{\bullet-}$ changes with distinct signals in living cells.

Thereafter, we employed the developed nanoprobe to study the dynamic changes of mitochondrial pH and $O_2^{\bullet-}$ in autophagy and the apoptosis process. Autophagy was first studied and induced by starvation conditions.[36] As shown in Figure 6a, the ratio signal of F_{Red}/F_{Purple} gradually increases with the change of time under starvation conditions. The pH values at different times are quantified by the intracellular pH curve. As shown in Figure 6b, the pH was gradually decreased with increasing time and the linear regression equation is $Y = -0.146x + 7.8846$. Using the absolute value of the slope k represents the kinetic constant of pH changes over time. We can see that the kinetic constant is 0.146 from 0 to 12 h under starvation conditions, demonstrating that the pH value gradually reduced during this time period. At the same time,

DOI: 10.1021/acsami.7b08223
ACS Appl. Mater. Interfaces 2017, 9, 27512−27521

the ratio of F_{Green}/F_{Purple} is almost unchanged from 0 to 4 h and increases gradually at 4−12 h (Figure 6a). As shown in Figure 6c, the linear regression equation is $Y = 0.00373x + 0.7236$ from 0 to 4 h and the linear regression equation is $Y = 0.0494x + 0.5762$ from 4 to 12 h. Similarly, the absolute value of the slope k represents the kinetic constant of the changes of $O_2^{\bullet-}$ level over time. The above results indicate that the kinetic constant is 0.00373 from 0 to 4 h, suggesting that the concentration of $O_2^{\bullet-}$ is almost unchanged in this period of time. The kinetic constant is 0.0494 from 4 to 12 h, indicating that the concentration of $O_2^{\bullet-}$ gradually increases in this period of time. Furthermore, we use acridine orange to stain the acidic vesicular organelles (AVOs), which are produced when autophagy happened. As shown in Figure S12, the red puncta dots (AVOs) were not observed from 0 to 4 h and gradually increased from 4 to 12 h under starved conditions. It suggested that the generation of AVOs fitted the evolution trend of $O_2^{\bullet-}$. The results are consistent with a previous report.[12] Therefore, these results implied that the pH value decreased and the $O_2^{\bullet-}$ level was almost unchanged at the initial stage of autophagy, whereas the pH continuously decreased and $O_2^{\bullet-}$ level increased at the late stage of autophagy.

Next, we applied the nanoprobe to explore the changes of pH and $O_2^{\bullet-}$ in the apoptosis process. The nanoprobe-treated HeLa cells were incubated with L-buthionine sulphoximine (BSO) for inducing cell apoptosis.[37] As shown in Figure 7a, the ratio of F_{Red}/F_{Purple} increases gradually over time in 0−4 h and the linear regression equation is $Y = -0.2036x + 7.9303$ (Figure 7b); the value of the kinetic constant k is 0.2036, indicating that the pH significantly decreased during this time period. From 4 to 12 h, the ratio of F_{Red}/F_{Purple} is almost unchanged and the linear regression equation is $Y = -0.014x + 7.1745$ (Figure 7b). The value of the kinetic constant is 0.014, indicating that the changes of pH are nearly constant in this time period. Then, $\Delta\psi_m$ was monitored using rhodamine 123. Fluorescence imaging results indicated that the fluorescence of rhodamine 123 gradually reduced from 0 to 4 h and then almost remained unchanged from 4 to 12 h (Figure S13), suggesting that the $\Delta\psi_m$ decreased gradually over time in 0−4 h and then remained nearly constant from 4 to 12 h. This demonstrated that the decreased $\Delta\psi_m$ was coincident with the reduction of mitochondrial pH, which was consistent with the previous report.[38] Moreover, the F_{Green}/F_{Purple} ratio signal increases gradually from 0 to 12 h (Figure 7a) and the linear regression equation is $Y = 0.0571x + 0.7185$ (Figure 7c). The value of the kinetic constant k is 0.0571, indicating that the concentrations of $O_2^{\bullet-}$ gradually increased in this period of time. Thus, these results suggested that the value of pH decreased and the $O_2^{\bullet-}$ level increased at the early stage of apoptosis, whereas the concentration of $O_2^{\bullet-}$ consistently increased and pH value was almost unchanged at the late stage of autophagy.

CONCLUSIONS

In conclusion, we develop a dual-ratiometric fluorescent nanoprobe for quantitatively detecting pH and $O_2^{\bullet-}$ in HeLa cells and further study the dynamics processes of pH and $O_2^{\bullet-}$ variations in autophagy and apoptosis processes. As expected, the nanoprobe can discriminatively and accurately report the variations of $O_2^{\bullet-}$ and pH. Fluorescence imaging experiments demonstrate that the nanoprobe is capable of precisely monitoring mitochondrial pH and $O_2^{\bullet-}$ changes in autophagy and apoptosis processes in HeLa cells by dual-ratiometric fluorescence imaging. By quantitative determination of kinetic constants of pH and $O_2^{\bullet-}$ changes, we found that the pH decreased and $O_2^{\bullet-}$ increased in both autophagy and apoptosis, but the dynamic changes of pH and $O_2^{\bullet-}$ are significantly different. In the early stage of autophagy, the pH value decreased, whereas $O_2^{\bullet-}$ remained unchanged. At the later stage of apoptosis, pH was unchanged and the concentration of $O_2^{\bullet-}$ increased. We expect that this work will not only offer valuable information for investigating $O_2^{\bullet-}$ and pH on regulation of cell function but also be helpful for studying the mechanisms of autophagy and apoptosis in human pathologies.

ASSOCIATED CONTENT

Supporting Information

The Supporting Information is available free of charge on the ACS Publications website at DOI: 10.1021/acsami.7b08223.

TEM image and dynamic light scattering histograms of the nanoprobe; standard linear calibration curves of RhB, DBZTC, Tpy-Cy, and TPP; stability of the nanoprobe; interference study; MTT; other quantitative data of the confocal fluorescence images (PDF)

AUTHOR INFORMATION

Corresponding Authors

*E-mail: lina@sdnu.edu.cn (N.L.).
*E-mail: tangb@sdnu.edu.cn (B.T.).

ORCID

Bo Tang: 0000-0002-8712-7025

Notes

The authors declare no competing financial interest.

ACKNOWLEDGMENTS

This work was supported by 973 Program (2013CB933800), National Natural Science Foundation of China (21390411, 21535004, 21422505, 21375081, and 21505087), and Natural Science Foundation for Distinguished Young Scholars of Shandong Province (JQ201503).

REFERENCES

(1) Cuervo, A. M.; Bergamini, E.; Brunk, U. T.; Dröge, W.; Ffrench, M.; Terman, A. Autophagy and Aging: the Importance of Maintaining "Clean" Cells. *Autophagy* **2005**, *1*, 131−140.

(2) Lum, J. J.; DeBerardinis, R. J.; Thompson, C. B. Autophagy in Metazoans: Cell Survival in the Land of Plenty. *Nat. Rev. Mol. Cell Biol.* **2005**, *6*, 439−448.

(3) Danial, N. N.; Korsmeyer, S. J. Cell Death: Critical Control Points. *Cell* **2004**, *116*, 205−219.

(4) Mizushima, N.; Levine, B.; Cuervo, A. M.; Klionsky, D. J. Autophagy Fights Disease through Cellular Self-Digestion. *Nature* **2008**, *451*, 1069−1075.

(5) Green, D. R.; Galluzzi, L.; Kroemer, G. Mitochondria and the Autophagy-Inflammation-Cell Death Axis in Organismal Aging. *Science* **2011**, *333*, 1109−1112.

(6) Clarke, P.; Tyler, K. L. Apoptosis in Animal Models of Virus-Induced Disease. *Nat. Rev. Microbiol.* **2009**, *7*, 144−155.

(7) Friedlander, R. M. Apoptosis and Caspases in Neurodegenerative Diseases. *N. Engl. J. Med.* **2003**, *348*, 1365−1375.

(8) Maiuri, M. C.; Zalckvar, E.; Kimchi, A.; Kroemer, G. Self-eating and Self-killing: Crosstalk between Autophagy and Apoptosis. *Nat. Rev. Mol. Cell Biol.* **2007**, *8*, 741−752.

(9) Matsuyama, S.; Reed, J. C. Mitochondria-Dependent Apoptosis and Cellular pH Regulation. *Cell Death Differ.* **2000**, *7*, 1155−1165.

(10) Li, L.; Chen, Y.; Gibson, S. B. Starvation-Induced Autophagy is Regulated by Mitochondrial Reactive Oxygen Species Leading to AMPK Activation. *Cell. Signalling* **2013**, *25*, 50−65.

DOI: 10.1021/acsami.7b08223
ACS Appl. Mater. Interfaces 2017, 9, 27512−27521

(11) Lee, M. H.; Park, N.; Yi, C.; Han, J. H.; Hong, J. H.; Kim, K. P.; Kang, D. H.; Sessler, J. L.; Kang, C.; Kim, J. S. Mitochondria-Immobilized pH-Sensitive off-on Fluorescent Probe. *J. Am. Chem. Soc.* **2014**, *136*, 14136−14142.
(12) Chen, Z.; Li, J.; Chen, X.; Cao, J.; Zhang, J.; Min, Q.; Zhu, J.-J. Single Gold@Silver Nanoprobes for Real-Time Tracing the Entire Autophagy Process at Single-Cell Level. *J. Am. Chem. Soc.* **2015**, *137*, 1903−1908.
(13) Matsuyama, S.; Llopis, J.; Deveraux, Q. L.; Tsien, R. Y.; Reed, J. C. Changes in Intramitochondrial and Cytosolic pH: Early Events that Modulate Caspase Activation during Apoptosis. *Nat. Cell Biol.* **2000**, *2*, 318−325.
(14) Antognelli, C.; Gambelunghe, A.; Talesa, V. N.; Muzi, G. Reactive Oxygen Species Induce Apoptosis in Bronchial Epithelial BEAS-2B Cells by Inhibiting the Antiglycation Glyoxalase I Defence: Involvement of Superoxide Anion, Hydrogen Peroxide and NF-κB. *Apoptosis* **2014**, *19*, 102−116.
(15) Casey, J. R.; Grinstein, S.; Orlowski, J. Sensors and Regulators of Intracellular pH. *Nat. Rev. Mol. Cell Biol.* **2010**, *11*, 50−61.
(16) Xia, M.-C.; Cai, L.; Zhang, S.; Zhang, X. Cell-Penetrating Peptide Spirolactam Derivative as a Reversible Fluorescent pH Probe for Live Cell Imaging. *Anal. Chem.* **2017**, *89*, 1238−1243.
(17) Li, N.; Wang, H.; Xue, M.; Chang, C.; Chen, Z.; Zhuo, L.; Tang, B. A Highly Selective and Sensitive Nanoprobe for Detection and Imaging of the Superoxide Anion Radical in Living Cells. *Chem. Commun.* **2012**, *48*, 2507−2509.
(18) Li, P.; Liu, L.; Xiao, H.; Zhang, W.; Wang, L.; Tang, B. A New Polymer Nanoprobe Based on Chemiluminescence Resonance Energy Transfer for Ultrasensitive Imaging of Intrinsic Superoxide Anion in Mice. *J. Am. Chem. Soc.* **2016**, *138*, 2893−2896.
(19) Hu, J. J.; Wong, N.-K.; Ye, S.; Chen, X.; Lu, M.-Y.; Zhao, A. Q.; Guo, Y.; Ma, A. C.-H.; Leung, A. Y.-H.; Shen, J.; Yang, D. Fluorescent Probe HKSOX-1 for Imaging and Detection of Endogenous Superoxide in Live Cells and in Vivo. *J. Am. Chem. Soc.* **2015**, *137*, 6837−6843.
(20) He, L.; Lin, W.; Xu, Q.; Wei, H. A Unique Type of Pyrrole-Based Cyanine Fluorophores with Turn-On and Ratiometric Fluorescence Signals at Different pH Regions for Sensing pH in Enzymes and Living Cells. *ACS Appl. Mater. Interfaces* **2014**, *6*, 22326−22333.
(21) Adams, S. R.; Harootunian, A. T.; Buechler, Y. J.; Taylor, S. S.; Tsien, R. Y. Fluorescence Ratio Imaging of Cyclic AMP in Single Cell. *Nature* **1991**, *349*, 694−697.
(22) Peng, X.; Yang, Z.; Wang, J.; Fan, J.; He, Y.; Song, F.; Wang, B.; Sun, S.; Qu, J.; Qi, J.; Yan, M. Fluorescence Ratiometry and Fluorescence Lifetime Imaging: Using a Single Molecular Sensor for Dual Mode Imaging of Cellular Viscosity. *J. Am. Chem. Soc.* **2011**, *133*, 6626−6635.
(23) Yang, Q.; Ye, Z.; Zhong, M.; Chen, B.; Chen, J.; Zeng, R.; Wei, L.; Li, H.-w.; Xiao, L. Self-Assembled Fluorescent Bovine Serum Albumin Nanoprobes for Ratiometric pH Measurement inside Living Cells. *ACS Appl. Mater. Interfaces* **2016**, *8*, 9629−9634.
(24) Shi, W.; Li, X.; Ma, H. A Tunable Ratiometric pH Sensor Based on Carbon Nanodots for the Quantitative Measurement of the Intracellular pH of Whole Cells. *Angew. Chem., Int. Ed.* **2012**, *51*, 6432−6435.
(25) Gao, X.; Ding, C.; Zhu, A.; Tian, Y. Carbon-Dot-Based Ratiometric Fluorescent Probe for Imaging and Biosensing of Superoxide Anion in Live Cells. *Anal. Chem.* **2014**, *86*, 7071−7078.
(26) Chen, Y.; Zhu, C.; Cen, J.; Bai, Y.; He, W.; Guo, Z. Ratiometric Detection of pH Fluctuation in Mitochondria with A New Fluorescein/Cyanine Hybrid Sensor. *Chem. Sci.* **2015**, *6*, 3187−3194.
(27) Zhou, Y.; Ding, J.; Liang, T.; Abdel-Halim, E. S.; Jiang, L.; Zhu, J.-J. FITC Doped Rattle-Type Silica Colloidal Particle-Based Ratiometric Fluorescent Sensor for Biosensing and Imaging of Superoxide Anion. *ACS Appl. Mater. Interfaces* **2016**, *8*, 6423−6430.
(28) Pan, W.; Wang, H.; Yang, L.; Yu, Z.; Li, N.; Tang, B. Ratiometric Fluorescence Nanoprobes for Subcellular pH Imaging with a Single-Wavelength Excitation in Living Cells. *Anal. Chem.* **2016**, *88*, 6743−6748.
(29) Stöber, W.; Fink, A.; Bohn, E. Controlled Growth of Monodisperse Silica Spheres in the Micron Size Range. *J. Colloid Interface Sci.* **1968**, *26*, 62−69.
(30) Gao, J. J.; Xu, K. H.; Tang, B.; Yin, L. L.; Yang, G. W.; An, L. G. Selective Detection of Superoxide Anion Radicals Generated from Macrophages by Using a Novel Fluorescent Probe. *FEBS J.* **2007**, *274*, 1725−1733.
(31) Tang, B.; Yu, F.; Li, P.; Tong, L.; Duan, X.; Xie, T.; Wang, X. A Near-Infrared Neutral pH Fluorescent Probe for Monitoring Minor pH Changes: Imaging in Living HepG2 and HL-7702 Cells. *J. Am. Chem. Soc.* **2009**, *131*, 3016−3023.
(32) Kobler, J.; Möller, K.; Bein, T. Colloidal Suspensions of Functionalized Mesoporous Silica Nanoparticles. *ACS Nano* **2008**, *2*, 791−799.
(33) Yu, Z.; Sun, Q.; Pan, W.; Li, N.; Tang, B. A Near-Infrared Triggered Nanophotosensitizer Inducing Domino Effect on Mitochondrial Reactive Oxygen Species Burst for Cancer Therapy. *ACS Nano* **2015**, *9*, 11064−11074.
(34) Zhou, Y.; Hileman, E. O.; Plunkett, W.; Keating, M. J.; Huang, P. Free Radical Stress in Chronic Lymphocytic Leukemia Cells and Its Role in Cellular Sensitivity to ROS-Generating Anticancer Agents. *Blood* **2003**, *101*, 4098−4104.
(35) Lee, M. H.; Han, J. H.; Lee, J. H.; Park, N.; Kumar, R.; Kang, C.; Kim, J. S. Two-Color Probe to Monitor a Wide Range of pH Values in Cells. *Angew. Chem., Int. Ed.* **2013**, *52*, 6206−6209.
(36) Tekirdag, K. A.; Korkmaz, G.; Ozturk, D. G.; Agami, R.; Gozuacik, D. MIR181A Regulates Starvation- and Rapamycin-Induced Autophagy through Targeting of ATG5. *Autophagy* **2013**, *9*, 374−385.
(37) Armstrong, J. S.; Steinauer, K. K.; Hornung, B.; Irish, J. M.; Lecane, P.; Birrell, G. W.; Peehl, D. M.; Knox, S. J. Role of Glutathione Depletion and Reactive Oxygen Species Generation in Apoptotic Signaling in a Human B Lymphoma Cell Line. *Cell Death Differ.* **2002**, *9*, 252−263.
(38) Matsuyama, S.; Llopis, J.; Deveraux, Q. L.; Tsien, R. Y.; Reed, J. C. Changes in Intramitochondrial and Cytosolic pH: Early Events That Modulate Caspase Activation during Apoptosis. *Nat. Cell Biol.* **2000**, *2*, 318−325.

DOI: 10.1021/acsami.7b08223
ACS Appl. Mater. Interfaces 2017, 9, 27512−27521